

# IMMP++: Isometric Motion Manifold Primitives with Parametric Curve Models

Yonghyeon Lee<sup>1</sup>

**Abstract**—The Motion Manifold Primitive (MMP) produces, for a given task, a continuous manifold of trajectories, each of which can successfully complete the task, addressing the challenge of high dimensionality in trajectory data. However, the discrete-time trajectory representations used in existing MMP methods lack important functionalities of movement primitives (e.g., temporal modulation, via-points modulation, etc.) found in other conventional methods that employ parametric curve representations. To address these limitations, we introduce *Motion Manifold Primitives++ (MMP++)*, which combines the advantages of the MMP and conventional methods by applying the MMP framework to the parametric curve representations. However, we observe that the performance of MMP++ can sometimes degrade significantly due to geometric distortion in the latent space — by distortion, we mean that similar motions are not located nearby in the latent space. To mitigate this issue, we propose *Isometric Motion Manifold Primitives++ (IMMP++)*, where the latent coordinate space preserves the geometry of the manifold. Experimental results with 2-DoF planar motions and 7-DoF robot arm tasks demonstrate that MMP++ and IMMP++ outperform existing methods, in some cases by a significant margin, while maintaining the advantages of parametric curve representations.

**Index Terms**—Movement Primitives, Manifold, Isometric Representation Learning, Autoencoders, Riemannian Geometry

## I. INTRODUCTION

Representation of basic motion skills through movement primitives continues to be a central focus in the literature on learning from demonstration [1]–[3]. When provided with a set of demonstration trajectories accomplishing a specific task, the main objective is to develop a model capable of generating diverse trajectories to perform the given task. The challenges arise from the small dataset size, high dimensionality of the trajectory data, and the multi-modality of data distribution, all of which impact the learning of movement primitives.

Adopting the motion manifold hypothesis [4], [5] – which assumes that a set of high dimensional trajectory data lies on some lower-dimensional manifold –, recent *Motion Manifold Primitives (MMP)* framework provides motion primitive models that can encode and generate, for a given task, a continuous manifold of trajectories each of which is capable of accomplishing the task [6], [7]. This framework has demonstrated promising results in addressing the aforementioned challenges, effectively reducing the data dimensionality and capturing multi-modality.

<sup>1</sup>Center for AI and Natural Sciences (CAINS), Korea Institute for Advanced Study (KIAS), Seoul, South Korea, ylee@kias.re.kr

This work has been submitted to the IEEE for possible publication. Copyright may be transferred without notice, after which this version may no longer be accessible.

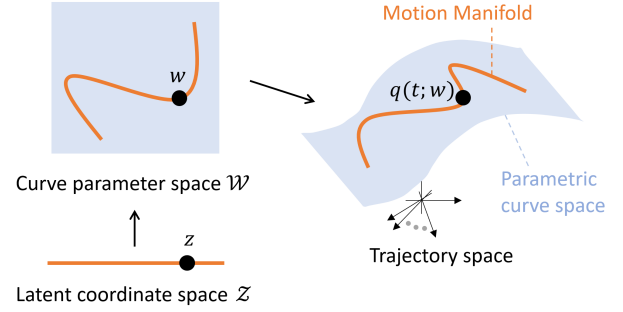


Fig. 1. *IMMP++*: A latent coordinate space  $\mathcal{Z}$  is mapped to a subspace of the curve parameter space  $\mathcal{W}$ ; the parameter space  $\mathcal{W}$  is mapped to a subspace of the infinite-dimensional trajectory space. The motion manifold and parametric curve space are visualized as a curve and surface, not because their actual dimensions are one and two, but only to indicate the relative size relationships of their dimensions.

However, these manifold-based models lack some of the desired functionalities of movement primitives found in other conventional methods (e.g., DMP [8], [9], ProMP [10], VMP [11]). These functionalities include: (i) temporal modulation to enable faster or slower execution of the movement, (ii) modulation of via-points (e.g., start and goal points) given new task constraints, and (iii) representation of rhythmic movements. The fundamental reason for the absence of such functions in the MMP framework is the use of discrete-time trajectory representation, while conventional movement primitives often employ parametric models with special structures to represent trajectories, e.g., linear basis function models: for a configuration space  $\mathcal{Q} = \mathbb{R}^n$ ,

$$q(t; w) = \sum_{i=1}^b \phi_i(t) w_i, \quad (1)$$

for  $\{\phi_i(t)\}_{i=1}^b$  is a set of some scalar-valued basis functions and  $w_i \in \mathbb{R}^n, i = 1, \dots, b$  are curve parameters.

By suitably designing a parametric curve model according to the given purpose, it is possible to implement the above-mentioned functionalities. In addition, using parametric curve representations has several other advantages. First, motions have bounded accelerations and jerks, avoiding sudden and abrupt changes. Second, the dimension of the parametric curve space – which is equal to the dimension of the parameter space – is generally much smaller than the dimension of the discrete-time trajectory data space, reducing the difficulty of the subsequent movement primitives learning problem.

Nevertheless, current parametric curve model-based methods continue to face challenges stemming from the high-

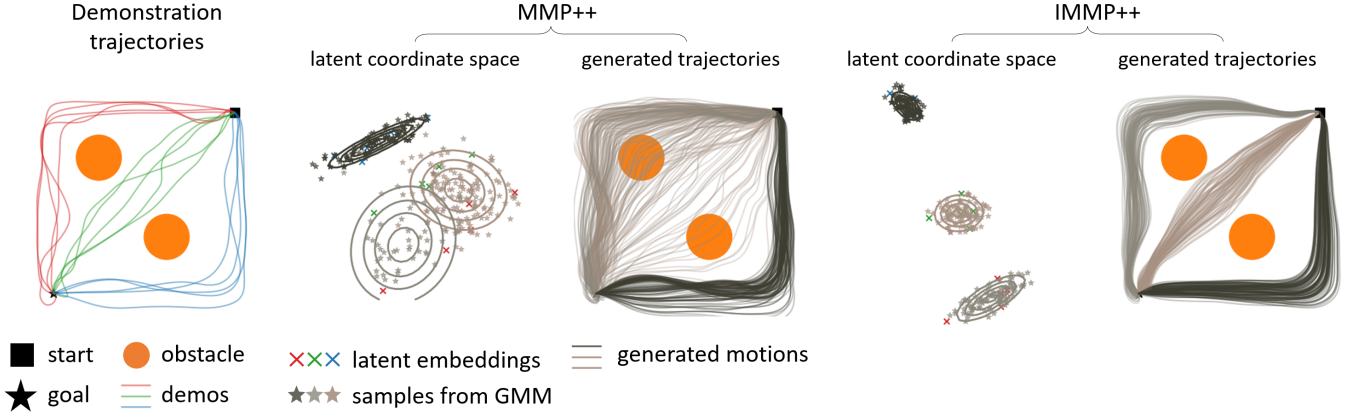


Fig. 2. *Left*: There are 15 demonstration trajectories (red, green, and blue trajectories) that travel from the start to the goal, avoiding the obstacle. *Middle and Right*: MMP++ and IMMP++ learn two-dimensional manifolds in the curve parameter space and produce two-dimensional latent coordinate spaces. Latent values of the demonstration trajectories are visualized in the latent coordinate spaces, marked as  $\times$ . GMMs of three components are fitted in the latent spaces, and the sampled points are visualized as stars  $*$ . The corresponding generated trajectories are also visualized.

dimensionality of the parameter space, resulting in less-than-desirable performance. Although the parameter space has a lower dimension than the trajectory space, it is still not sufficiently low to enable accurate learning of movement primitives. To address this, we propose applying the MMP framework to the parametric curve representations of trajectories, thus simultaneously tackling the challenge of dimensionality and achieving the desired functionalities, denoted as *MMP++* (see Fig. 1).

The vanilla MMP++, a naive application of the MMP framework to the curve parameter space, however, often results in a *geometrically distorted* latent coordinate space – where similar motion data are not positioned close to each other –, leading to a generation of motions that violate the task constraint. For example, consider an example shown in Fig. 2. We learn a two-dimensional manifold and its latent coordinate space, by using the red, green, and blue demonstration trajectories and their parametric curve representations. Then we fit a Gaussian Mixture Model (GMM) using the latent values of the trajectories. As illustrated in Fig. 2 (*Middle*), due to the geometric distortion in the latent coordinate space, the same color trajectories are not located close enough to each other. Consequently, the red and green latent points are not correctly clustered by the GMM, and many of the generated motions collide with the obstacle, failing to accomplish the task.

In this paper, adopting the isometric regularization method from [12], we propose to learn a *geometry-preserving latent coordinate space*, so that similar trajectories can be located nearby in the latent space. To employ this method in our context, we need to specify a *Riemannian metric* for the curve parameter space that serves as the basis for determining the notion of closeness in the parameter space. We propose a *CurveGeom Riemannian metric* for the curve parameter space, that reflects the geometry of the trajectory space, given a curve model  $q(t; w)$  that satisfies some mild regularity conditions. We call this framework *Isometric Motion Manifold Primitives++ (IMMP++)*; see Fig. 2 (*Right*).

In our experiments, we use affine curve models, similar to

those in ProMP [10] and VMP [11], and assume Euclidean configuration spaces. This induces constant CurveGeom metrics and lead to simpler implementations of the isometric regularization. Experiments involving 2-DoF planar obstacle-avoiding motions and 7-DoF collision-free motions of a robot arm confirm that our manifold-based methods, MMP++ and IMMP++, outperform existing methods.

## II. RELATED WORKS

### A. Movement Primitives

Methods for movement primitives can be roughly divided into two categories: (i) dynamical system-based approaches, such as dynamic movement primitives [8], [9], [13]–[16] and stable dynamical system [17]–[22]; and (ii) modeling trajectory distribution [6], [7], [10], [11], [23]. Our work falls into the second category. The trajectory modeling methods can be further divided into two subcategories. First, a parametric curve model is used to explicitly impose an inductive bias on the generated trajectory and has natural adaptability in temporal modulation and constraint changes [10], [11], [23]. The second involves learning a low-dimensional trajectory manifold and fitting a distribution model in the latent coordinate space to overcome the high-dimensionality issue [6], [7]. Our work combines the advantage of using the parametric curve model and that of the manifold learning to develop adaptable and accurate motion primitives.

### B. Manifold Learning and Latent Space Distortion

An autoencoder framework and its variants have received a lot of attention as effective methods to learn the manifold and its coordinate chart simultaneously, including but not limited to [12], [24]–[32]. Of particular relevance to our paper, a geometric perspective on autoencoders has been eloquently presented in [5]. In our paper, a significant aspect of concern is the presence of the geometric distortion within the latent space of the autoencoder, as highlighted in [4], [5], [12], [29], [33]. A recent regularization method [12] has developed a method

to find the one that minimizes the geometric distortion, i.e., preserves the geometry of the data manifold and the latent coordinate space. While Euclidean metric is assumed in [12], in this work, we propose to use a pullback Riemannian metric for the curve parameter space that reflects the geometry of the curve space.

### III. GEOMETRIC PRELIMINARIES

In this section, we review some basic concepts in differential geometry that serve as cornerstones for our method. We refer to standard differential geometry textbooks for more details [34], [35].

#### A. Riemannian Manifolds

A smooth manifold  $\mathcal{M}$  equipped with a positive-definite inner product on the tangent space at each point is called a *Riemannian manifold*, and the family of inner products is called a *Riemannian metric*. Given an  $m$ -dimensional Riemannian manifold  $\mathcal{M}$  and its local coordinates  $x \in \mathbb{R}^m$  – when using local coordinates, we implicitly assume there exists a local coordinate map  $\psi : \mathbb{R}^m \rightarrow \mathcal{U} \subset \mathcal{M}$  –, the Riemannian metric at  $x$  can be expressed as an  $m \times m$  positive-definite matrix denoted by  $G(x) \in \mathbb{R}^{m \times m}$ . This defines several geometric notions on  $\mathcal{M}$ , such as lengths, angles, and volumes. For example, given an infinitesimal displacement vector  $dx \in \mathbb{R}^m$ , its squared length is defined as follows:

$$ds^2 = dx^T G(x) dx = \sum_{i,j=1}^m g_{ij}(x) dx^i dx^j, \quad (2)$$

where  $\{g_{ij}(x)\}$  is an index notation of the matrix  $G(x)$  and  $dx = (dx^1, \dots, dx^m)$ .

#### B. Immersion and Embedding

Consider two differentiable manifolds, an  $m$ -dimensional manifold  $\mathcal{M}$  and  $n$ -dimensional manifold  $\mathcal{N}$ , with their respective coordinates  $x \in \mathbb{R}^m$  and  $y \in \mathbb{R}^n$ . A differentiable mapping  $f : \mathcal{M} \rightarrow \mathcal{N}$  is an *immersion* if its differential is an injective function at every point in  $\mathcal{M}$ . Representing the mapping in local coordinates as  $f : \mathbb{R}^m \rightarrow \mathbb{R}^n$ , equivalently,  $f$  is an immersion if its Jacobian matrix

$$J(x) := \frac{\partial f}{\partial x}(x) \in \mathbb{R}^{n \times m} \quad (3)$$

has constant rank equal to  $\dim(\mathcal{M}) = m$ . Intuitively, for  $f$  to be an immersion, the output manifold dimension  $n$  must be greater or equal to the dimension of  $\mathcal{M}$ . A smooth *embedding* is an injective immersion  $f : \mathcal{M} \rightarrow \mathcal{N}$  such that  $\mathcal{M}$  is diffeomorphic to its image  $f(\mathcal{M}) \subset \mathcal{N}$ <sup>1</sup>. Specifically, when the domain manifold is compact, a smooth embedding is equivalent to an injective immersion. Then,  $f(\mathcal{M})$  is called an *embedded manifold* in  $\mathcal{N}$ .

<sup>1</sup>A manifold  $\mathcal{A}$  is diffeomorphic to another manifold  $\mathcal{B}$  if there exists a differentiable map between  $\mathcal{A}$  and  $\mathcal{B}$  such that its inverse exists and is differentiable as well.

#### C. Riemannian Geometry of Parametric Curves

In this paper, we are particularly interested in Riemannian geometry of manifold of parametric curves. This section introduces how to define a Riemannian metric for the parametric curve manifold.

Let  $\mathcal{M}$  be an  $m$ -dimensional Riemannian manifold with its local coordinates  $x \in \mathbb{R}^m$  and Riemannian metric  $G(x)$ . Consider a smooth curve in  $\mathcal{M}$  expressed as  $x : [0, T] \rightarrow \mathbb{R}^m$  in coordinates, where its velocity norm is defined as  $\|\dot{x}\| := \sqrt{\dot{x}^T G(x) \dot{x}}$ . The space of all smooth curves is considered an infinite-dimensional function space  $\mathcal{X}$  with an inner product defined as follows:  $\langle v, w \rangle_x := \int_0^T v(t)^T G(x(t)) w(t) dt$  for two square-integrable functions  $v, w : [0, T] \rightarrow \mathbb{R}^m$  (i.e.,  $\mathcal{X}$  is a Hilbert space).

Of particular relevance to this paper is a parametric curve  $x(t; w)$  where  $w \in \mathcal{W}$  denotes the parameter of the curve and  $\mathcal{W} \subset \mathbb{R}^n$ . Consider the set of all parametric curves  $\mathcal{X}_{\mathcal{W}} := \{x(\cdot; w) \in \mathcal{X} \mid w \in \mathcal{W}\}$ . This space is a  $n$ -dimensional smooth manifold under the following conditions:

**Proposition 1.** Suppose a curve  $x(t; w)$  is smooth in both  $t$  and  $w$  and  $x(t; \cdot) : \mathcal{W} \rightarrow \mathcal{X}$  is injective, i.e., if  $x(t; w_1) = x(t; w_2)$  for all  $t \in [0, T]$ , then  $w_1 = w_2$ . Let  $w = (w^1, \dots, w^n)$  and  $v = (v^1, \dots, v^n) \in \mathbb{R}^n$ , if

$$\sum_{i=1}^n \frac{\partial x(t; w)}{\partial w^i} v^i = 0 \implies v = 0 \quad (4)$$

for all  $w \in \mathcal{W}$  and  $\mathcal{W}$  is compact, then  $\mathcal{X}_{\mathcal{W}}$  is an  $n$ -dimensional smooth manifold.

*Proof.* A smooth map  $x(t; \cdot) : \mathcal{W} \rightarrow \mathcal{X}$  is an injective immersion by (4). Since  $\mathcal{W}$  is compact, the mapping is an embedding (i.e.,  $\mathcal{X}_{\mathcal{W}}$  is an embedded manifold in  $\mathcal{X}$ ).  $\square$

Given a parametric curve manifold  $\mathcal{X}_{\mathcal{W}}$  embedded in  $\mathcal{X}$ , the inner product  $\langle \cdot, \cdot \rangle_x$  in  $\mathcal{X}$  can be naturally projected into  $\mathcal{X}_{\mathcal{W}}$ . This leads to – by treating  $\mathcal{W}$  as a local coordinate space for  $\mathcal{X}_{\mathcal{W}}$  – the Riemannian metric in  $\mathcal{X}_{\mathcal{W}}$  expressed in the parameter space  $\mathcal{W}$ , denoted by  $H(w) = \{h_{ij}(w)\}$ . Specifically, the squared length of an infinitesimal displacement  $dw \in \mathbb{R}^n$  is

$$\begin{aligned} ds^2 &= \sum_{i,j} h_{ij}(w) dw^i dw^j \\ &= \int_0^T \left\langle \sum_i \frac{\partial x(t; w)}{\partial w^i} dw^i, \sum_j \frac{\partial x(t; w)}{\partial w^j} dw^j \right\rangle_x dt \\ &= \sum_{i,j} \left( \int_0^T \frac{\partial x(t; w)^T}{\partial w^i} G(x(t; w)) \frac{\partial x(t; w)}{\partial w^j} dt \right) dw^i dw^j. \end{aligned} \quad (5)$$

Therefore,

$$H(w) = \int_0^T \left( \frac{\partial x(t; w)}{\partial w} \right)^T G(x(t; w)) \frac{\partial x(t; w)}{\partial w} dt, \quad (6)$$

where  $\frac{\partial x(t; w)}{\partial w} \in \mathbb{R}^{m \times n}$ . This method of metric construction follows the standard procedure in differential geometry. A similar procedure can be found in the construction of Fisher information Riemannian metrics in statistical manifolds [32], [36].

#### D. Isometry and Coordinate-Invariant Distortion Measure

Consider two Riemannian manifolds, an  $m$ -dimensional manifold  $\mathcal{M}$  with local coordinates  $x \in \mathbb{R}^m$  and metric  $G(x)$  and an  $n$ -dimensional manifold  $\mathcal{N}$  with local coordinates  $y \in \mathbb{R}^n$  and metric  $H(y)$ . And let  $f : \mathbb{R}^m \rightarrow \mathbb{R}^n$  be a differentiable mapping between two manifolds expressed in local coordinates.

We call  $f$  an *isometry* if it preserves geometric structures between two spaces, i.e., preserves distances, angles, and volumes. Specifically, let  $J(x) = \frac{\partial f}{\partial x}(x)$ , if

$$G(x) = J(x)^T H(f(x)) J(x) \quad (7)$$

at  $x$ , then  $f$  is called a local isometry at  $x$  (to see why, compare  $dx^T G(x) dx$  and  $dy^T H(y) dy$  where  $dy = J(x) dx$ ). If this condition is satisfied at all points in  $\mathcal{M}$ , then  $f$  is a (global) isometry.

Sometimes, it is too stringent to find an isometry between two spaces and better to ignore the scale of distances [12]. A mapping  $f$  that satisfies the relaxed condition

$$G(x) = c J(x)^T H(f(x)) J(x) \quad (8)$$

for all  $x$  and for some positive scalar  $c$  is called a *scaled isometry*. It preserves, angles and scaled distances.

There is a family of coordinate-invariant Riemannian *distortion measures*, each of which is a functional of a mapping  $f$  that measures how far  $f$  from being an isometry [37]. Let  $\lambda_i$  be eigenvalues of  $J^T H J G^{-1}$ . One example is

$$\int_{\mathcal{M}} \|\lambda_i(x) - 1\|^2 \sqrt{\det G(x)} dx. \quad (9)$$

This measure is coordinate-invariant<sup>2</sup>, and note that if  $\lambda_i(x) = 1$  for all  $x$ , then the measure is zero and  $f$  is an isometry.

A family of *relaxed distortion measures* quantifies how far  $f$  from being a scaled isometry [12] within the support of a positive finite measure  $\nu$  in  $\mathcal{M}$ . One of them is

$$\int_{\mathcal{M}} \left\| \frac{\lambda_i(x)}{\frac{1}{\nu(\mathcal{M})} \int_{\mathcal{M}} \frac{1}{\sum_{i=1}^m \lambda_i(x)} d\nu(x)} - 1 \right\|^2 d\nu(x). \quad (10)$$

This measure is coordinate-invariant, and note that if  $\lambda_i(x) = c$  for all  $x$  in the support of  $\nu$  for some positive scalar  $c$ , then the measure is zero and  $f$  is a scaled isometry in  $\nu$  (i.e., equation (8) is satisfied at all points in the support of  $\nu$ ).

Given a probability measure  $P$  in  $\mathcal{M}$ , restricting the relaxed distortion measure (10) to the support of  $P$  and removing the additive constant, it is proportional to

$$\mathcal{R}(f; P) := \frac{\mathbb{E}_{x \sim P} [\text{Tr}((J^T H J G^{-1})^2)]}{\mathbb{E}_{x \sim P} [\text{Tr}(J^T H J G^{-1})]^2}. \quad (11)$$

Given this trace-based expression, we can employ the Hutchinson stochastic trace estimator, i.e.,  $\text{Tr}(A) = \mathbb{E}_{v \sim \mathcal{N}(0, I)} [v^T A v]$ , which facilitates an efficient implementation of isometric regularization. Further details can be found in [5], [7].

<sup>2</sup>To see why, consider a pair of coordinate transformations  $\psi : x \mapsto x'$  and  $\phi : y \mapsto y'$ . Let  $\Psi = \frac{\partial \psi}{\partial x}$  and  $\Phi = \frac{\partial \phi}{\partial y}$ , then the Riemannian metrics transform via  $G \mapsto \Psi^{-T} G \Psi^{-1}$  and  $H \mapsto \Phi^{-T} H \Phi^{-1}$ , while the Jacobian transforms via  $J \mapsto \Phi J \Psi^{-1}$ . Therefore,  $J^T H J G^{-1} \mapsto \Psi^{-T} J^T H J G^{-1} \Psi^T$  and the eigenvalues remain unchanged.

#### IV. ISOMETRIC MOTION MANIFOLD PRIMITIVES++

In this section, we first propose Motion Manifold Primitives++ (MMP++), applying the MMP framework to the parametric curve representations. Then we adopt the isometric regularization technique [12] with our proposed CuveGeom Riemannian metrics, and propose Isometric Motion Manifold Primitives++ (IMMP++).

We begin by introducing notations used throughout. We will consider an  $n$ -dimensional Riemannian configuration manifold  $\mathcal{Q}$  with its coordinates  $q \in Q \subset \mathbb{R}^n$  and the metric  $G(q) = \{g_{ij}(q)\}$ . We use a phase variable  $\tau \in [0, 1]$ , and our main subject of interest is a parametric curve model

$$q : [0, 1] \times \mathcal{W} \rightarrow Q \text{ s.t. } q(\tau, w) \in Q. \quad (12)$$

Then, given any monotonically increasing function with time  $\tau(t)$ , a timed-trajectory  $q(\tau(t); w)$  can be constructed with a desired velocity profile  $\frac{d}{dt} q(\tau(t); w) = \dot{\tau}_t \frac{\partial}{\partial \tau} q(\tau; w)$ . This is called a temporal modulation.

Specifically, we focus on a particular class of curve models, an affine curve model, that is expressed as follows:

$$q(\tau; w) = \psi(\tau) + w\phi(\tau), \quad (13)$$

where  $\psi(\tau) \in \mathbb{R}^n$ ,  $\phi(\tau) \in \mathbb{R}^B$ , and  $w \in \mathbb{R}^{n \times B}$ . This class includes models from ProMP [10] and VMP [11]. In VMP,  $\psi(\tau)$  is referred to as an elementary trajectory, and  $w\phi(\tau)$  is termed a shape modulation.

We assume that we are provided with multiple demonstration trajectories for a given task, each of which is a sequence of time-configuration pairs  $((t_1, q_1), \dots, (t_L, q_L))$ . In the pre-processing step, we fit each demonstration trajectory to the affine curve model (13) and find  $w$ . Specifically, we set  $\tau_{\text{linear}}(t) = \frac{t}{t_L}$  and consider  $\Delta_i := q_i - \psi(\tau_{\text{linear}}(t_i))$ . Then, we want to find  $w$  that best fits the trajectory, i.e.,  $\min_w \sum_{i=1}^L \|\Delta_i - w\phi(\tau_{\text{linear}}(t_i))\|$ . Assuming  $L > B$ , there is a closed-form solution:

$$w^* = \Delta \Phi^T (\Phi \Phi^T)^{-1}, \quad (14)$$

where the data matrix  $\Delta = (\Delta_1, \dots, \Delta_L) \in \mathbb{R}^{n \times L}$  and basis matrix  $\Phi = (\phi(\tau_{\text{linear}}(t_1)), \dots, \phi(\tau_{\text{linear}}(t_L))) \in \mathbb{R}^{B \times L}$ .

In the subsequent sections, we assume that we are given curve parameters fitted to the demonstration trajectories, denoted by  $\{w_1, \dots, w_N\}$  where  $w_i \in \mathbb{R}^{n \times B}$  is a curve parameter fitted to an  $i$ -th trajectory.

##### A. Motion Manifold Primitives++

Adopting [6], [7], we use an autoencoder framework to learning manifold and its coordinate. An autoencoder consists of an encoder  $g : \mathcal{W} \rightarrow \mathcal{Z}$  and a decoder  $f : \mathcal{Z} \rightarrow \mathcal{W}$ , where  $\mathcal{W} = \mathbb{R}^{n \times B}$  is the curve parameter space and  $\mathcal{Z} = \mathbb{R}^m$  is a latent coordinate space. There two mappings are optimized to minimize the following standard autoencoder reconstruction loss:

$$\frac{1}{L} \sum_{i=1}^L \|w_i - f(g(w_i))\|_F^2, \quad (15)$$

where  $\|\cdot\|_F$  is the Frobenius norm.



Minimizing (15) makes  $\{w_i\}_{i=1}^N$  approximately lie on the image of the decoder function  $f$ . As discussed in section III-B, if  $f$  is injective, the Jacobian of  $f$  is  $m$  everywhere, and  $f$  is diffeomorphic to its image, then the image of the decoder can be considered as an  $m$ -dimensional manifold embedded in  $\mathcal{W}$ . Then, the mappings  $g, f$  with  $\mathcal{Z}$  take the role of the coordinate chart. Consequently, an autoencoder can be interpreted as learning motion manifold and its coordinates, simultaneously.

In practice, we approximate  $g$  and  $f$  using deep neural networks with smooth activation functions. By setting  $m$  sufficiently low, much lower than  $\dim(\mathcal{W}) = nB$ , empirical results imply that  $f$  converges to satisfy the above conditions without enforcing them. However, choosing a large  $m$  may drop the rank of the Jacobian of  $f$  [5].

Once  $f, g$  are fitted, we train a latent space distribution using the encoded data  $\{g(w_i)\}_{i=1}^N$ . To capture the multi-modality of the distribution, we use a Gaussian Mixture Model (GMM), yet any other distribution fitting methods can be used. We call this framework *Motion Manifold Primitives++ (MMP++)*, where ‘++’ is added to distinguish it from vanilla MMP that uses discrete-time trajectory representations.

### B. Isometric Regularization

The MMP++ often produces a geometrically distorted latent coordinate space  $\mathcal{Z}$ . Adopting [12], we would like to minimize the distortion between  $\mathcal{Z}$  and  $f(\mathcal{Z}) \subset \mathcal{W}$  by adding the relaxed distortion measure (11) of the decoder mapping  $f : \mathcal{Z} \rightarrow \mathcal{W}$  to the reconstruction loss function.

We consider the latent space  $\mathcal{Z}$  as a Riemannian manifold assigned with the identity metric  $I \in \mathbb{R}^{m \times m}$ , i.e., an  $m$ -dimensional Euclidean space. To apply the isometric regularization [12], we should be able to interpret the output space  $\mathcal{W}$  as a local coordinate space for the embedded manifold  $\mathcal{X}_{\mathcal{W}} = \{\psi(\tau) + w\phi(\tau) \in \mathcal{X} \mid w \in \mathcal{W}\}$  (see section III-C). The space  $\mathcal{X}_{\mathcal{W}}$  is an  $nB$ -dimensional smooth manifold, if  $\phi_1(\tau), \dots, \phi_B(\tau)$  are linearly independent:

**Proposition 2.** *Suppose  $\phi_1(\tau), \dots, \phi_B(\tau)$  are linearly independent, i.e., if  $a_1\phi_1(\tau) + a_2\phi_2(\tau) + \dots + a_d\phi_d(\tau) = 0$  for all  $\tau \in [0, 1]$ , then  $(a_1, \dots, a_d) = 0$ . Then, the affine curve model (13) satisfies the injective immersion condition in Proposition 1.*

*Proof.* Suppose  $\psi(\tau) + w_1\phi(\tau) = \psi(\tau) + w_2\phi(\tau)$  for all  $\tau$ , which implies that  $(w_1 - w_2)\phi(\tau) = \sum_{j=1}^B (w_1 - w_2)^{ij} \phi_j(\tau) = 0$  for all  $\tau$  and  $i$ . By the linearity,  $w_1 = w_2$ ; the injectivity is proved. Now, suppose  $\sum_{i,j} \frac{\partial q(\tau; w)}{\partial w^{ij}} v^{ij} = 0$ , which implies that  $\sum_j v^{ij} \phi_j(\tau) = 0$  for all  $\tau$  and  $i$ . Similarly, by the linearity,  $v = 0$ ; thus the mapping  $w \mapsto w\phi(\tau)$  is an immersion.  $\square$

In existing movement primitives [10], [11], one of the standard methods for constructing  $\phi(\tau)$  involves normalizing scalar-valued functions  $b_i(\tau), i = 1, \dots, B$ :  $\phi_i(\tau) = b_i(\tau) / \sum_{j=1}^B b_j(\tau)$ . With this construction, if  $\{b_i\}$  is linearly independent and  $\sum_j b_j(\tau) > 0$  for all  $\tau$ , then  $\{\phi_i\}$  is linearly independent as well. We can construct such  $\{b_i\}$  with the following proposition:

**Proposition 3.** (Corollary of Proposition 4.3. in [38]) *Let  $K : \mathbb{R} \times \mathbb{R} \rightarrow \mathbb{R}$  be a positive function and  $\{c_1, c_2, \dots, c_B\}$  be a*

*finite set of mutually distinct points. Define  $b_i(\tau) = K(\tau, c_i)$ . Then  $\{b_i\}$  is linearly independent if and only if the matrix  $(K(c_i, c_j))_{i,j=1,\dots,B}$  is positive definite.*

Consider the most standard choice of  $b_i(\tau)$  for stroke-based movements, the Gaussian basis functions  $b_i^G(\tau) := \exp(-\frac{(\tau - c_i)^2}{2h})$  where  $h$  defines the width of basis and  $c_i$  the center for the  $i$ -th basis. According to Proposition 3, if  $\{c_1, c_2, \dots, c_B\}$  is mutually distinct, then  $\{b_i^G\}$  is linearly independent, because Gaussian kernel is positive definite.

For a smooth manifold  $\mathcal{X}_{\mathcal{W}}$ , we can now define a Riemannian metric expressed in coordinates  $w \in \mathcal{W}$  using equation (6). Since our parameter  $w \in \mathbb{R}^{n \times B}$  is a matrix and has two indices  $\{w^{ij}\}$ , the Riemannian metric has four indices  $h_{ijkl}(w)$  such that

$$ds^2 = \sum_{i,k=1}^n \sum_{j,l=1}^B h_{ijkl}(w) dw^{ij} dw^{kl} \quad (16)$$

for  $dw \in \mathbb{R}^{n \times B}$ . Accordingly, we define a CurveGeom Riemannian metric in  $\mathcal{W}$  as follows:

**Definition 1.** *A CurveGeom Riemannian metric for  $\mathcal{X}_{\mathcal{W}}$  expressed in  $\mathcal{W}$  is*

$$h_{ijkl}(w) = \int_0^1 \frac{\partial q(\tau; w)^T}{\partial w^{ij}} G(q(\tau; w)) \frac{\partial q(\tau; w)}{\partial w^{kl}} d\tau \quad (17)$$

for  $i, k = 1, \dots, n$  and  $j, l = 1, \dots, B$ .

Given an affine curve model, the metric further simplifies to the following expression:

**Proposition 4.** *Suppose  $q(\tau; w) = \psi(\tau) + w\phi(\tau)$ , then the CurveGeom Riemannian metric is*

$$h_{ijkl}(w) = \int_0^1 \phi_j(\tau) g_{ik}(q(\tau; w)) \phi_l(\tau) d\tau, \quad (18)$$

for  $i, k = 1, \dots, n$  and  $j, l = 1, \dots, B$ .

*Proof.* Let us denote by  $q = (q^1, \dots, q^n)$ . Then,  $\frac{\partial q^a(\tau; w)}{\partial w^{ij}} = \frac{\partial}{\partial w^{ij}} (\sum_b w^{ab} \phi_b) = \sum_b \delta_i^a \delta_j^b \phi_b = \delta_i^a \phi_j$ . Therefore, the metric is  $h_{ijkl} = \int \sum_{a,b} g_{ab} \delta_i^a \phi_j \delta_k^b \phi_l d\tau = \int g_{ik} \phi_j \phi_l d\tau$ .  $\square$

Now, we can compute the relaxed distortion measure of the decoder mapping  $f : \mathcal{Z} \rightarrow \mathcal{W}$  using equation (11). Since the metric for  $\mathcal{Z}$  is the identity, we only need to compute  $J^T H J$ . Unlike the case in equation (11), the Jacobian of our decoder  $f = (f^{ij})_{i=1,\dots,n,j=1,\dots,B}$  is not a matrix, but has three indices  $\frac{\partial f^{ij}}{\partial z^a}$  where  $a = 1, \dots, m$ . Therefore, instead of  $J^T H J$ , we can write it as follows:

$$\bar{h}_{ab}(z) = \sum_{i,k=1}^n \sum_{j,l=1}^B \left( \frac{\partial f^{ij}}{\partial z^a}(z) \right)^T h_{ijkl}(f(z)) \frac{\partial f^{kl}}{\partial z^b}(z), \quad (19)$$

where  $\frac{\partial f^{ij}}{\partial z^a}(z) \in \mathbb{R}^{1 \times m}$ . We let  $\{\bar{h}_{ab}(z)\}$  be an index notation of an  $m \times m$  matrix  $\bar{H}(z)$ . If  $\bar{H}(z) = cI$  for some positive scalar  $c$  for all  $z$ , then  $f$  is a scaled isometry.

We consider a latent space probability measure  $P$  and finally define the relaxed distortion measure as

$$\mathcal{R}(f; P) := \frac{\mathbb{E}_{z \sim P} [\text{Tr}(\bar{H}(z)^2)]}{\mathbb{E}_{z \sim P} [\text{Tr}(\bar{H}(z))]^2}. \quad (20)$$

Following [12], sampling from  $P$  is done by  $\delta z_i + (1 - \delta)z_j$  where  $\delta$  is uniformly sampled from  $[-\eta, 1 + \eta]$  (we set  $\eta = 0.2$  throughout) and  $z_i = g(w_i)$  and  $z_j = g(w_j)$  with  $w_i, w_j \sim \{w_i\}_{i=1}^N$ . The final loss function is

$$\frac{1}{L} \sum_{i=1}^L \|w_i - f(g(w_i))\|^2 + \alpha \mathcal{R}(f; P), \quad (21)$$

where  $\alpha$  is a regularization coefficient. Together with the density model fitted in the latent coordinate space, we call this framework *Isometric Motion Manifold Primitives++* (IMMP++),

As a special case, if  $\mathcal{Q}$  is Euclidean space, i.e.,  $g_{ij}(w)$  is equal to the Kronecker delta  $\delta_{ij}$ , then the metric formula and isometric regularization term can be further simplified. Plugging it into equation (18), the metric is simplified to

$$h_{ijkl} = \delta_{ik} \int_0^1 \phi_j(\tau) \phi_l(\tau) d\tau. \quad (22)$$

We note that it does not depend on  $w$ ; therefore, we do not need to compute it in every iteration of the gradient descent during autoencoder training. This greatly reduces the computational cost in isometric regularization. Specifically, the matrix  $\bar{H}(z)$  becomes

$$\bar{h}_{ab}(z) = \sum_{i=1}^n \left( \frac{\partial f^i}{\partial z}(z) \right)^T \Phi \frac{\partial f^i}{\partial z}(z), \quad (23)$$

where  $f^i = (f^{i1}, \dots, f^{iB}) \in \mathbb{R}^B$ ,  $\frac{\partial f^i}{\partial z}(z) \in \mathbb{R}^{B \times m}$ , and  $\Phi = (\int_0^1 \phi_j(\tau) \phi_l(\tau) d\tau)_{j,l=1,\dots,B} \in \mathbb{R}^{B \times B}$  is constant.

## V. EXPERIMENTS

Throughout, we assume Euclidean configuration space  $\mathcal{Q}$  and focus on examples with fixed initial and final points  $q_i, q_f \in \mathcal{Q}$ , therefore we use the via-point affine curve model from VMP [11]:

$$q(\tau; w) = (1 - \tau)q_i + \tau q_f + w\phi(\tau), \quad (24)$$

where  $\phi_i(\tau) = \tau(1 - \tau) b_i^G(\tau) / \sum_j b_j^G(\tau)$  (it is trivial to show the linear independence of  $\phi_i$ ; see Proposition 3). To give hard constraints of initial and final points to  $q(\tau; w)$ , we multiply  $\tau(1 - \tau)$  to the original basis term from [11].

We compare MMP++, IMMP++, and VMP [11]. We utilize Gaussian Mixture Models (GMMs) to fit latent density models for MMP++ and IMMP++ unless otherwise specified. While the distribution of  $w$  is assumed to be Gaussian in vanilla VMP, it has limitations in capturing multi-modal distributions. To ensure a fair comparison, we also implement VMP with GMM. When sampling new trajectories from fitted distributions, we reject the samples with likelihood values lower than the threshold value  $\eta$  – where  $\eta$  is set to be the minimum value among the likelihood values of the training trajectories.

### A. Planar Obstacle-Avoiding Motions

We consider three different environments with different numbers of obstacles and obstacle-avoiding trajectories; see Env1, Env2, and Env3 in Fig. 3. The number of total training trajectories for each environment setting is 10, 15, and 20,

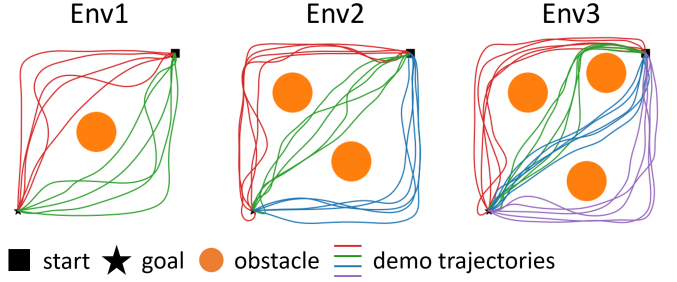


Fig. 3. Three environments with training demonstration trajectories.

TABLE I  
AVERAGES AND STANDARD DEVIATIONS OF THE SUCCESS RATES WITH 5 TIMES RUN WITH DIFFERENT RANDOM SEEDS; THE HIGHER THE BETTER. THE BEST RESULTS ARE MARKED IN BOLD.

	Env1	Env2	Env3
VMP (Gaussian)	76.42 $\pm$ 1.34	65.76 $\pm$ 1.60	38.24 $\pm$ 1.18
VMP (GMM)	97.12 $\pm$ 0.51	97.52 $\pm$ 0.30	98.14 $\pm$ 0.24
MMP++ (ours)	99.48 $\pm$ 0.38	88.58 $\pm$ 0.60	97.76 $\pm$ 1.46
IMMP++ (ours)	<b>100.00 <math>\pm</math> 0.00</b>	<b>99.90 <math>\pm</math> 0.12</b>	<b>99.22 <math>\pm</math> 0.19</b>

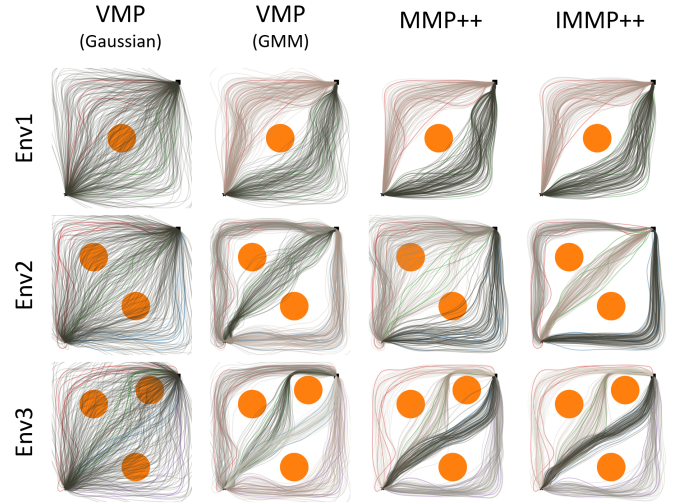


Fig. 4. Trajectories generated by trained models. The GMM component numbers are 2, 3, and 4 for Env1, Env2, and Env3, respectively (samples from the same GMM component are assigned the same color).

respectively. The number of basis  $B = 20$  for  $\phi(\tau)$ . In MMP++ and IMMP++, the latent space dimension is search among 2, 3, 4, and 5. The number of GMM components is set to be 2, 3, and 4 for Env1, Env2, and Env3, respectively. A generated trajectory is considered successful if it does not collide with the obstacles.

As shown in Table I and Fig. 4, the IMMP++ performs the best compared to the other methods. Sometimes, MMP++ fails significantly because GMM fits wrong clusters due to the geometric distortions in the latent coordinate spaces; see Fig. 2 for example latent spaces of MMP+ and IMMP++.

### B. 7-DoF Robot Arm Collision-Free Motions

In this section, we consider collision-free point-to-point motions of a 7-DoF Franka Emika Panda robot arm in an

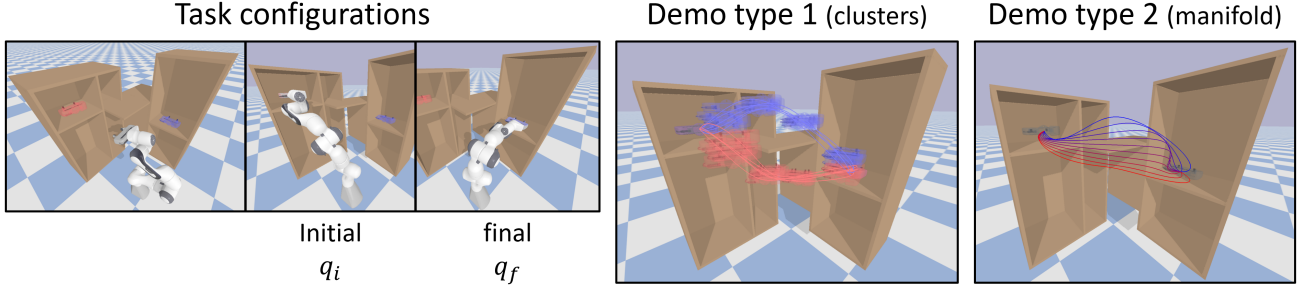


Fig. 5. *Left*: A 7-DoF robot arm needs to move from the joint configuration  $q_i$  to  $q_f$  without colliding to the environment. *Right*: Two types of demonstration trajectories, where 7-dimensional joint space trajectories are given as demonstration data (only the end-effector’s SE(3) or  $\mathbb{R}^3$  trajectories are visualized).

environment shown in Fig. 5 (*Left*). Two types of demonstration trajectories are given, each with 10 joint space trajectories – in Fig. 5 (*Right*), SE(3) and  $\mathbb{R}^3$  forward kinematics results of them are visualized for simplicity –, where the initial and final configurations are identical as  $q_i$  and  $q_f$  in Fig. 5 (*Left*). In the demo type 1, there are two clusters of trajectories, whereas in the demo type 2 a set of trajectories forms an 1-dimensional manifold, a trajectory manifold embedded in the trajectory space. The number of basis  $B = 20$  for  $\phi(\tau)$ . In MMP++ and IMMP++, the latent space dimensions are 2. The number of GMM components is 2. Exceptionally, for MMP++ and IMMP++ applied to the demo type 2, we use the Kernel Density Estimator (KDE) instead of the GMM (we will provide the reason later).

Table II shows the averages and standard deviations of the success rates. Overall, MMP++ and IMMP++ show the best performances. In particular, VMPs show far inferior results than our manifold-based methods given a manifold of demonstrations in the demo type 2. Fig. 6 shows the two-dimensional latent spaces of the manifold-based methods. For demo type 1, the distance between clusters in the latent space of IMMP++ is greater than that in the latent space of MMP++. Even though MMP++ successfully captures correct clusters in this particular dataset, for more complex datasets, it is more likely to fail in capturing correct clustering structures.

For demo type 2, we note that two-dimensional encoded latent points form an one-dimensional manifold; it should be considered as a single connected manifold component. Given this manifold support, we found that it is sub-optimal to use the GMM for fitting a distribution. Hence, we use a non-parametric method, KDE, that can more accurately estimate our latent space density function:

$$p(z) = \frac{1}{N} \sum_{i=1}^N \frac{1}{2\pi|H_i|^{1/2}} \exp\left(-\frac{(z - z_i)^T H_i^{-1} (z - z_i)}{2}\right), \quad (25)$$

where  $\{z_i\}_{i=1}^N$  is the set of encoded latent points and  $H_i, i = 1, \dots, N$  are positive-definite matrices. Let  $K(z_i, z_k) = \exp(-\|z_i - z_k\|^2/h)$ ; for this example, we construct  $H_i = \Sigma_i^2$  where

$$\Sigma_i = \frac{\sum_{k=1}^N K(z_i, z_k)(z_i - z_k)(z_i - z_k)^T}{\sum_{k=1}^N K(z_i, z_k)}. \quad (26)$$

One may ask if using such a non-parametric method in the curve parameter space  $\mathcal{W}$  directly can lead to a better perfor-

TABLE II  
AVERAGES AND STANDARD DEVIATIONS OF THE SUCCESS RATES WITH 5 TIMES RUN WITH DIFFERENT RANDOM SEEDS; THE HIGHER THE BETTER. THE BEST RESULTS ARE MARKED IN BOLD.

Demo	VMP (Gaussian)	VMP (GMM)	MMP++ (ours)	IMMP++ (ours)
type 1	46.1 $\pm$ 4.37	97.1 $\pm$ 1.66	98.6 $\pm$ 0.20	<b>99.5 <math>\pm</math> 0.77</b>
type 2	79.4 $\pm$ 2.94	83.0 $\pm$ 3.78	<b>99.3 <math>\pm</math> 0.68</b>	98.2 $\pm$ 0.68

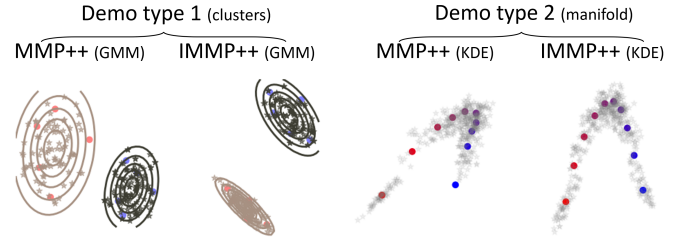


Fig. 6. The two-dimensional latent spaces of our manifold-based methods (MMP++ and IMMP++) are illustrated (circular points are encoded points and star-shaped points are generated samples). Demonstration trajectories in Fig. 5 (*Right*) are encoded into these latent spaces, with colors indicating correspondence (e.g., a red trajectory is encoded into a red point).

mance than using GMM. Unfortunately, this is challenging due to the high-dimensional nature of  $\mathcal{W}$ . It is worth noting that this approach is feasible because we utilize a sufficiently low-dimensional latent space. We can see that the samples in the IMMP++ latent space are well-placed on the one-dimensional manifold with a little less noise than MMP++.

## VI. CONCLUSION AND DISCUSSION

We have proposed a new family of movement primitives based on the motion manifold hypothesis, Motion Manifold Primitives++ (MMP++), which combines the advantage of the existing MMP and that of the conventional parametric curve representations-based methods, resulting in higher motion generation accuracy and adaptability. Further, to address the geometric distortion issue in MMP++, we have introduced a CurveGeom Riemannian metric for the parametric curve space and presented Isometric Motion Manifold Primitives++ (IMMP++). In this approach, the latent space preserves the geometric structure of the motion manifold, leading, in some cases, to significantly improved density fitting results in the latent space. We have demonstrated the advantages of using our manifold-based methods, not only in terms of performance

but also by highlighting that the low-dimensional nature of the latent space enables the use of non-parametric density estimation methods such as KDE, which is not feasible in the high-dimensional curve parameter space.

**Limitations and Future Directions:** One limitation of the current version of our methods is that the generated motions are not guaranteed to satisfy given constraints. If we have explicit equations for constraints that can be expressed in the latent space as  $C(z) \leq 0$  for latent coordinates  $z \in \mathcal{Z}$ , we can perform a simple optimization to modify a generated trajectory to meet the constraints. For instance, given an initial sample  $z_0 \sim p(z)$ , we can solve the following constrained optimization:

$$\min_z 1 \text{ s.t. } C(z) \leq 0, \log p(z) \geq \eta \quad (27)$$

where  $\eta$  is the minimum log-likelihood value among the training latent points. Since we start from a good initial point  $z_0$  and thanks to the low-dimensionality of the latent space, this optimization process is expected to converge rapidly.

#### ACKNOWLEDGMENTS

Yonghyeon Lee was the beneficiary of an individual grant from CAINS supported by a KIAS Individual Grant (AP092701) via the Center for AI and Natural Sciences at Korea Institute for Advanced Study.

#### REFERENCES

- [1] B. D. Argall, S. Chernova, M. Veloso, and B. Browning, “A survey of robot learning from demonstration,” *Robotics and autonomous systems*, vol. 57, no. 5, pp. 469–483, 2009.
- [2] M. Saveriano, F. J. Abu-Dakka, A. Kramberger, and L. Peternel, “Dynamic movement primitives in robotics: A tutorial survey,” *arXiv preprint arXiv:2102.03861*, 2021.
- [3] Z. Zhu and H. Hu, “Robot learning from demonstration in robotic assembly: A survey,” *Robotics*, vol. 7, no. 2, p. 17, 2018.
- [4] G. Arvanitidis, L. K. Hansen, and S. Hauberg, “Latent space oddity: on the curvature of deep generative models,” *arXiv preprint arXiv:1710.11379*, 2017.
- [5] Y. Lee, “A geometric perspective on autoencoders,” *arXiv preprint arXiv:2309.08247*, 2023.
- [6] M. Noseworthy, R. Paul, S. Roy, D. Park, and N. Roy, “Task-conditioned variational autoencoders for learning movement primitives,” in *Conference on robot learning*. PMLR, 2020, pp. 933–944.
- [7] B. Lee, Y. Lee, S. Kim, M. Son, and F. C. Park, “Equivariant motion manifold primitives,” in *7th Annual Conference on Robot Learning*, 2023.
- [8] S. Schaal, P. Mohajerian, and A. Ijspeert, “Dynamics systems vs. optimal control—a unifying view,” *Progress in brain research*, vol. 165, pp. 425–445, 2007.
- [9] A. J. Ijspeert, J. Nakanishi, H. Hoffmann, P. Pastor, and S. Schaal, “Dynamical movement primitives: learning attractor models for motor behaviors,” *Neural computation*, vol. 25, no. 2, pp. 328–373, 2013.
- [10] A. Paraschos, C. Daniel, J. R. Peters, and G. Neumann, “Probabilistic movement primitives,” *Advances in neural information processing systems*, vol. 26, 2013.
- [11] Y. Zhou, J. Gao, and T. Asfour, “Learning via-point movement primitives with inter-and extrapolation capabilities,” in *2019 IEEE/RSJ International Conference on Intelligent Robots and Systems (IROS)*. IEEE, 2019, pp. 4301–4308.
- [12] Y. Lee, S. Yoon, M. Son, and F. C. Park, “Regularized autoencoders for isometric representation learning,” in *International Conference on Learning Representations*, 2022.
- [13] A. Pervez, A. Ali, J.-H. Ryu, and D. Lee, “Novel learning from demonstration approach for repetitive teleoperation tasks,” in *2017 IEEE World Haptics Conference (WHC)*. IEEE, 2017, pp. 60–65.
- [14] Y. Fanger, J. Umlauft, and S. Hirche, “Gaussian processes for dynamic movement primitives with application in knowledge-based cooperation,” in *2016 IEEE/RSJ International Conference on Intelligent Robots and Systems (IROS)*. IEEE, 2016, pp. 3913–3919.
- [15] J. Umlauft, Y. Fanger, and S. Hirche, “Bayesian uncertainty modeling for programming by demonstration,” in *2017 IEEE International Conference on Robotics and Automation (ICRA)*. IEEE, 2017, pp. 6428–6434.
- [16] A. Pervez, Y. Mao, and D. Lee, “Learning deep movement primitives using convolutional neural networks,” in *2017 IEEE-RAS 17th international conference on humanoid robotics (Humanoids)*. IEEE, 2017, pp. 191–197.
- [17] S. M. Khansari-Zadeh and A. Billard, “Learning stable nonlinear dynamical systems with gaussian mixture models,” *IEEE Transactions on Robotics*, vol. 27, no. 5, pp. 943–957, 2011.
- [18] K. Neumann, A. Lemme, and J. J. Steil, “Neural learning of stable dynamical systems based on data-driven lyapunov candidates,” in *2013 IEEE/RSJ International Conference on Intelligent Robots and Systems*. IEEE, 2013, pp. 1216–1222.
- [19] K. Neumann and J. J. Steil, “Learning robot motions with stable dynamical systems under diffeomorphic transformations,” *Robotics and Autonomous Systems*, vol. 70, pp. 1–15, 2015.
- [20] C. Blocher, M. Saveriano, and D. Lee, “Learning stable dynamical systems using contraction theory,” in *2017 14th International Conference on Ubiquitous Robots and Ambient Intelligence (URAI)*. IEEE, 2017, pp. 124–129.
- [21] V. Sindhvani, S. Tu, and M. Khansari, “Learning contracting vector fields for stable imitation learning,” *arXiv preprint arXiv:1804.04878*, 2018.
- [22] J. Z. Kolter and G. Manek, “Learning stable deep dynamics models,” *Advances in neural information processing systems*, vol. 32, 2019.
- [23] Y. Huang, L. Roza, J. Silvério, and D. G. Caldwell, “Kernelized movement primitives,” *The International Journal of Robotics Research*, vol. 38, no. 7, pp. 833–852, 2019.
- [24] Y. Lee, H. Kwon, and F. Park, “Neighborhood reconstructing autoencoders,” *Advances in Neural Information Processing Systems*, vol. 34, pp. 536–546, 2021.
- [25] D. P. Kingma and M. Welling, “Auto-encoding variational bayes,” *arXiv preprint arXiv:1312.6114*, 2013.
- [26] A. Creswell, Y. Mohamied, B. Sengupta, and A. A. Bharath, “Adversarial information factorization,” *arXiv preprint arXiv:1711.05175*, 2017.
- [27] S. Rifai, P. Vincent, X. Muller, X. Glorot, and Y. Bengio, “Contractive auto-encoders: Explicit invariance during feature extraction,” in *Proceedings of the 28th international conference on international conference on machine learning*, 2011, pp. 833–840.
- [28] Y. Lee and F. C. Park, “On explicit curvature regularization in deep generative models,” *arXiv preprint arXiv:2309.10237*, 2023.
- [29] P. Nazari, S. Damrich, and F. A. Hamprecht, “Geometric autoencoders—what you see is what you decode,” 2023.
- [30] S. Yoon, Y.-K. Noh, and F. Park, “Autoencoding under normalization constraints,” in *International Conference on Machine Learning*. PMLR, 2021, pp. 12 087–12 097.
- [31] C. Jang, Y. Lee, Y.-K. Noh, and F. C. Park, “Geometrically regularized autoencoders for non-euclidean data,” in *The Eleventh International Conference on Learning Representations*.
- [32] Y. Lee, S. Kim, J. Choi, and F. Park, “A statistical manifold framework for point cloud data,” in *International Conference on Machine Learning*. PMLR, 2022, pp. 12 378–12 402.
- [33] H. Shao, A. Kumar, and P. Thomas Fletcher, “The riemannian geometry of deep generative models,” in *Proceedings of the IEEE Conference on Computer Vision and Pattern Recognition Workshops*, 2018, pp. 315–323.
- [34] M. P. Do Carmo and J. Flaherty Francis, *Riemannian geometry*. Springer, 1992, vol. 6.
- [35] M. Fecko, *Differential geometry and Lie groups for physicists*. Cambridge university press, 2006.
- [36] S.-i. Amari, *Information geometry and its applications*. Springer, 2016, vol. 194.
- [37] C. Jang, Y.-K. Noh, and F. C. Park, “A riemannian geometric framework for manifold learning of non-euclidean data,” *Advances in Data Analysis and Classification*, vol. 15, no. 3, pp. 673–699, 2021.
- [38] V. I. Paulsen and M. Raghupathi, *An introduction to the theory of reproducing kernel Hilbert spaces*. Cambridge university press, 2016, vol. 152.